Chinese Chemical Letters 33 (2022) 390–393

Contents lists available at ScienceDirect

Chinese Chemical Letters

journal homepage: www.elsevier.com/locate/cclet

Highly selective conversion of methane to ethanol over $CuFe_2O_4$-carbon nanotube catalysts at low temperature

Xinquan Shen[a,b], Dan Wu[a], Xian-Zhu Fu[a,*], Jing-Li Luo[a,*]

[a] Shenzhen Key Laboratory of Polymer Science and Technology, Guangdong Research Center for Interfacial Engineering of Functional Materials, College of Materials Science Engineering, Shenzhen University, Shenzhen 518071, China
[b] Key Laboratory of Optoelectronic Devices and Systems of Ministry of Education and Guangdong Province, College of Optoelectronic Engineering, Shenzhen University, Shenzhen 518060, China

ARTICLE INFO

Article history:
Received 24 April 2021
Revised 14 June 2021
Accepted 6 July 2021
Available online 16 July 2021

Keywords:
Methane
Ethanol
High selectivity
Synergistic effect
Catalysis

ABSTRACT

Conversion of methane into liquid alcohol such as ethanol at low temperature in a straight, selective and low energy consumption process remains a topic of intense scientific research but a great challenge. In this work, $CuFe_2O_4$/CNT composite is successfully synthesized *via* a facile co-reduction method and used as catalysts to selectively oxidize methane. At a low temperature of 150 °C, methane is directly converted to ethanol in a single process on the as-prepared $CuFe_2O_4$/CNT composite with high selectivity. A mechanism is also proposed for the significant methane selective oxidation performance of the $CuFe_2O_4$/CNT composite catalysts.

The high availability of methane (CH_4) from conversional and unconventional reserves calls for the development of efficient methods for its conversion. Among the various oxidation products from CH_4 conversion, ethanol is an important chemical raw material that has numerous applications such as chemical feedstock, sanitizer, additive and liquid fuel [1-5]. Conversion of CH_4 to ethanol is of great significance for clean and sustainable development. In the conventional processes, CH_4 is firstly reformed into syngas and then converted to ethanol by Fischer-Tropsch synthesis [3-7]. Unfortunately, this process of CH_4 reforming requires high temperature (typically > 800 °C), resulting in high energy consumption [8]. In this regard, many catalysts (MIL-53 [9], Cu-mordenite zeolite [10], Fe-ZSM-5 [11], $Ln_2Zr_2O_7$ [12]) are developed to lower the reaction temperature for the CH_4 conversion. However, selective conversion of CH_4 at relatively low temperature is still challenging.

From the perspective of thermodynamically and kinetics, CH_4 can be oxidized to oxygenates at low temperature [13]. According to the calculation of Gibbs free energy, the highest theoretical conversion is near 33% when the equilibrium is reached at room temperature. However, the best selectivity was obtained after maximum conversion is near 5% [14]. The major challenge in the direct selective oxidation of CH_4 is resulted from its large bond dissociation energy (435 kJ/mol), which hinders C-H cleavage reactions. In terms of most of the intermediate products, this high activation barrier means the subsequent oxidation of intermediates is favorable over CH_4 oxidation. For example, with the C-H bond energy of 393 kJ/mol, methanol is easier to be oxidized to stable products of over oxidation (*i.e.*, CO or CO_2) than to oxidize CH_4 itself [2,15,16]. As a result, a variety of catalysts such as Cu-Fe/ZSM-5 [8], Au-Pd [17], Au/SiO_2 [18] are attempted to converse CH_4 into oxygenates with high selectivity by suppressing the formation of undesirable over-oxidation products. However, only C_1 compounds as main products were obtained in current CH_4 thermodynamic catalytic processes. Therefore, it is of significance to seek advanced heterogeneous catalyst to enable efficient C–H activation and C–C coupling.

Interestingly, methanotrophic bacteria in nature demonstrate that one-step oxidation of methane to high-added-value products is feasible using methane monooxygenase enzymes. The nature of their active sites provides information for the development of synthetic methane to oxygenates oxidation catalysts [19-21].

Inspired by the methanotrophic bacteria which can one-step oxidize CH_4 to high-added-value products using Cu and/or Fe active species in the enzymes [20,21], we develop a facile approach to load $CuFe_2O_4$ on the carbon nanotubes (CNTs). The resultant $CuFe_2O_4$/CNT is highly active to convert CH_4 at low temperature of 150 °C. Particularly, 82% selectivity of ethanol can be achieved in a synergetic combination of coordination of Cu and Fe species

* Corresponding authors.
E-mail addresses: xz.fu@szu.edu.cn (X.-Z. Fu), jingli.luo@ualberta.cn (J.-L. Luo).

https://doi.org/10.1016/j.cclet.2021.07.019
1001-8417/

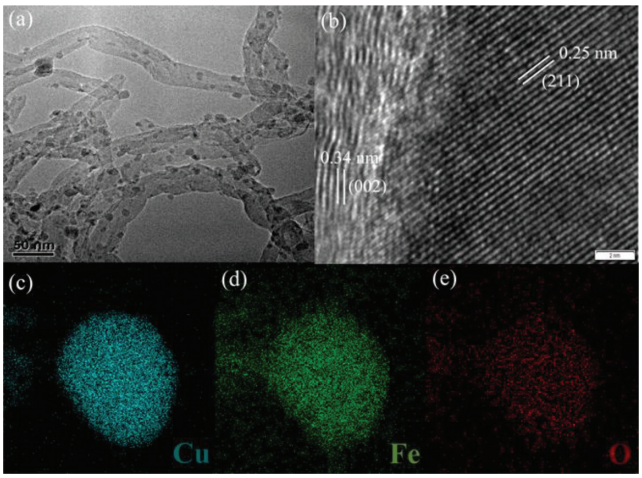

Fig. 1. TEM images and EDX maps in $CuFe_2O_4$/CNT.

in $CuFe_2O_4$ and strong interaction to CNT support. This work provides valuable insights for CH_4 conversion into value-added fuels using non-noble catalysts operating at mild conditions.

In this work, we prepared $CuFe_2O_4$ catalysts *via* a co-reduction following by heat treatment method (details see Supporting information) to improve the selectivity of ethanol from CH_4. As shown in Fig. S1 in Supporting information, the diffraction peaks in X-ray diffraction (XRD) pattern can be indexed to copper ferrite ($CuFe_2O_4$, JCPDS No. 34-0425) [22,23]. The sample obtained in the absence of Cu and Fe source is identified as Fe_2O_3 and CuO, respectively. To get more detailed information on the crystalline structure of the composite, the transmission electron microscopy (TEM) images of $CuFe_2O_4$/CNT at different magnifications are displayed in Fig. 1. The low-resolution image (Fig. 1a) confirms that the $CuFe_2O_4$ particles with diameter of 10–20 nm are well dispersed among the CNT substrate. As displayed in Fig. 1b, two sets of the lattice fringes are observed for the $CuFe_2O_4$/CNT catalyst. The interplanar distance of 0.25 nm corresponds to the (211) plane of $CuFe_2O_4$ (JCPDS No. 34-0425), while the fringe spacing of 0.34 nm corresponds to the (002) lattice plane of CNT [24]. The seamless contact of the lattice fringes suggests that $CuFe_2O_4$ nanoparticles are tightly attached to the CNT to form $CuFe_2O_4$/CNT composite. The intimate contact usually leads to interaction between metal oxides and support [25-28]. The uniform distributions of Cu, Fe and O elements in the Energy-dispersive detector spectra (Figs. 1c–e) further confirm the formation of $CuFe_2O_4$ nanoparticles. X-ray photoelectron spectroscopy (XPS) is performed to obtain the information on the surface composition and chemical states of $CuFe_2O_4$/CNT catalysts. The signals of Cu, Fe, O and C elements are detected in the survey spectra of $CuFe_2O_4$/CNT (Fig. S2a in Supporting information). For the high resolution Fe 2p XPS spectra of $CuFe_2O_4$/CNT (Fig. S2b in Supporting information), two peaks at the binding energies of 711.7 eV and 713.5 eV in the realm of Fe $2p_{3/2}$ correspond to tetrahedral Fe^{3+} ions and octahedral Fe^{3+} ions, respectively [29-33]. Concurrently, the peaks referred to the tetrahedral Fe^{3+} ions (724.8 eV) and octahedral Fe^{3+} ions (726.6 eV) are also found in the Fe $2p_{1/2}$ region. Similarly, in the spectra of Cu 2p (Fig. S2c in Supporting information) for $CuFe_2O_4$/CNT, the peaks at binding energies of 953.02 eV and 933.26 eV are assigned to Cu^{2+} on octahedral sites, while the peaks at binding energies of 955.15 eV and 935.46 eV are assigned to Cu^{2+} on tetrahedral sites [23,31-34]. Moreover, the spectral profile of $CuFe_2O_4$/CNT shows 0.3 eV and 0.2 eV shift to the higher binding energies, compared to Fe_2O_3/CNT and CuO/CNT, respectively. The results demonstrate that the chemical states of Fe and Cu in $CuFe_2O_4$/CNT are totally different from those in Fe_2O_3 and CuO.

The as-prepared catalysts are employed to oxidize CH_4 at low temperature of 150 °C. As shown in Fig. 2a, ethanol is the main oxidation products for CH_4 oxidation on $CuFe_2O_4$/CNT catalysts with a major proportion of 82%, accompanying with methanol, acetone and formic acid with selectivity of 7.3%, 7.3% and 3.2%, respectively, which is identified by gas chromatographymass spectrometry (GC-MS) (Fig. S3 in Supporting information). Comparatively, these four oxidation products are also detected for Fe_2O_3/CNT and CuO/CNT (Fig. S4a in Supporting information). In addition, over-oxidation products CO_x converted from CH_4 are also found for Fe_2O_3/CNT. However, the selectivity of ethanol on Fe_2O_3/CNT and CuO/CNT is 13% and 44%, respectively, which is much lower than $CuFe_2O_4$/CNT (Fig. 2b). Additionally, CNT is inactive for ethanol generation. Thus, the metal species (Fe_2O_3, CuO and $CuFe_2O_4$) are the active phase for ethanol formation from CH_4. Given that the configuration environment of Cu and Fe species in $CuFe_2O_4$/CNT is totally different from those in Fe_2O_3/CNT and CuO/CNT, the physical mixtures of Fe_2O_3/CNT and CuO/CNT with the same metal weight percent are also used for CH_4 selective oxidation. Compared to $CuFe_2O_4$/CNT, the physically mixed catalysts exhibit inferior ethanol selectivity (10%) with more over-oxidation products CO_x (19%) (Fig. 2b and Fig. S4a in Supporting information). The superior catalytic performance of $CuFe_2O_4$/CNT demonstrate that the coordination of Cu and Fe species in $CuFe_2O_4$/CNT composite contributes to the highly selective ethanol generation from CH_4 oxidation.

Fig. 3a shows the H_2-temperature programmed reduction (TPR) profiles of $CuFe_2O_4$/CNT, $CuFe_2O_4$, Fe_2O_3/CNT and CuO/CNT. There are two peaks at around 174 and 288 °C for CuO/CNT, which are assigned to the reduction of the Cu^{2+} to Cu^+, Cu^+ to Cu^0, respectively [35,36]. There are three peaks at around 323, 499 and 568 °C for Fe_2O_3/CNT. The peak at around 323 °C is the reduction of Fe_2O_3 into Fe_3O_4, while the broad peaks at around 499 and 568 °C are due to the subsequent multiple reduction of Fe_3O_4 to FeO and Fe [30,37,38]. Comparatively, there are four peaks at around 188, 248, 395 and 501 °C for $CuFe_2O_4$/CNT. The peak at around 188 °C can be ascribed to the reduction of $CuFe_2O_4$ to Cu^0 and Fe_2O_3 phases [37], while the peaks at around 248, 395 and 501 °C are due to the further reduction of Fe_2O_3 to Fe_3O_4, Fe_3O_4 to FeO and Fe, respectively [38]. Compared to Fe_2O_3/CNT, the Fe species in the $CuFe_2O_4$/CNT composite exhibit lower reduction temperature, demonstrating a synergistic effect between Cu and Fe species within the $CuFe_2O_4$/CNT composite, in which Cu promoted the reduction of Fe at a lower temperature [35-39]. The TPR profile changes induced by the interaction between Cu and Fe species indicate that the enhanced oxygen transfer properties and a better electron acceptor for $CuFe_2O_4$/CNT [40,41]. Moreover, the spectra profile of $CuFe_2O_4$/CNT is also different from that of $CuFe_2O_4$, demonstrating the interaction between $CuFe_2O_4$ particles and CNT supports [42,43], which is consistent with TEM results. Thus, the enhanced redox property of $CuFe_2O_4$/CNT composite would accelerate the activation of CH_4 and further formation of ethanol. From the above analysis, the Cu and Fe species in $CuFe_2O_4$/CNT composite remarkably affect the ethanol selectivity. Accordingly, the yield of ethanol over the $CuFe_2O_4$/CNT is calculated as 2.02%. The CH_4 conversion efficiency increases with the higher concentration of Fe species, so the Fe is reasoned to be the main active center for CH_4 oxidation. There are over-oxidation products of CO and CO_2 using Fe_2O_3/CNT as catalysts. The addition of Cu species can decrease the concentration of generated hydroxyl radicals, which are of strong oxidative ability to oxidize the carbon-containing intermediates. This is consistent with the electron paramagnetic resonance (EPR) radical trapping studies on Fe/ZSM-5 and Cu/ZSM-5 [8]. The intermediates during the CH_4 oxidation process is probed by *in situ* infrared (IR) spectroscopy. As shown in Fig. 3b, no stable surface species are observed over CNT (Fig. S5 in Supporting information), confirming that the CNT alone is inert for CH_4 conversion.

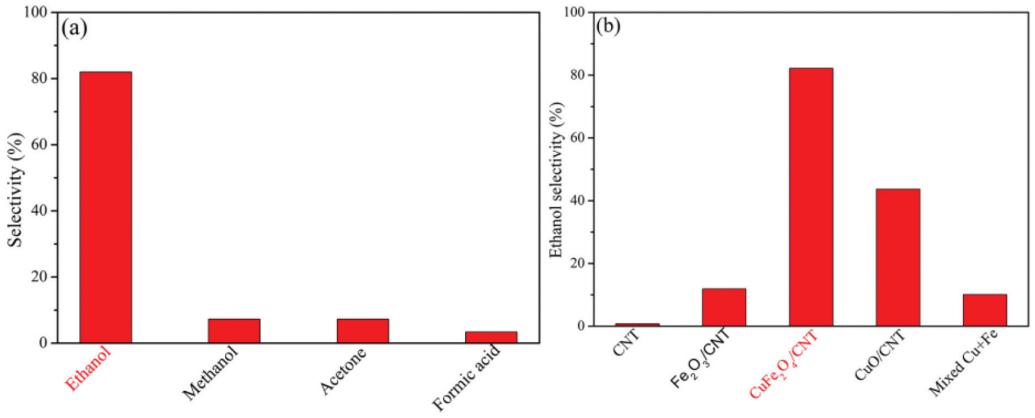

Fig. 2. (a) Selectivity of products formed during reaction of methane over $CuFe_2O_4$/CNT; (b) Ethanol selectivity of all catalysts for the oxidation of methane.

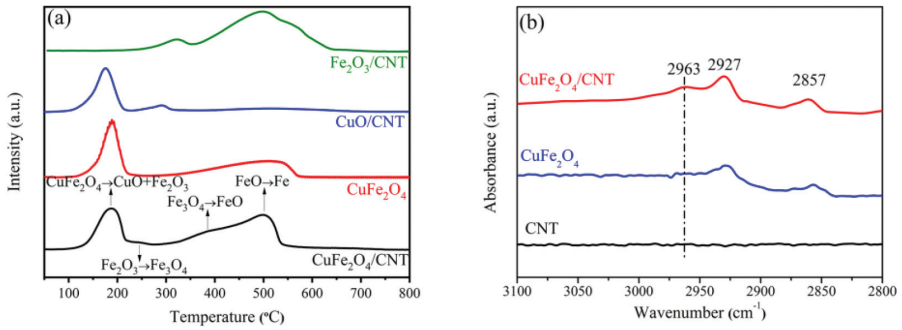

Fig. 3. (a) H_2-TPR spectra of catalysts; (b) FT-IR spectra of intermediates formed in CH_4 oxidation.

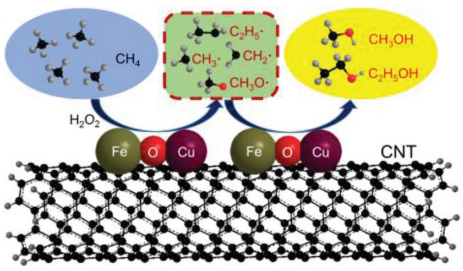

Fig. 4. Reaction paths on $CuFe_2O_4$/CNT for the oxidation of methane.

Two bands at around 2927 and 2857 cm^{-1} are observed for the $CuFe_2O_4$ catalyst, which is attributed to asymmetric and symmetric CH_2 stretching modes, respectively [44-47]. Comparatively, one more peak at around 2963 cm^{-1} corresponding to CH_3 stretching modes is found for $CuFe_2O_4$/CNT [47,48]. This confirms that the strong interaction between $CuFe_2O_4$ and CNTs facilitates the CH_4 activation.

Accordingly, the possible reaction paths for the formation of ethanol from CH_4 over the $CuFe_2O_4$/CNT composite catalysts is proposed in Fig. 4. The hydroxyl radicals are usually believed to precipitate in CH_4 oxidation process [8]. On the one hand, CH_4 is firstly activated mainly by Fe species in $CuFe_2O_4$. The surface CH_3 and CH_2 species are formed and then coupled to form longer alkyl and alkoxy chains speedily, further leading to the formation of oxygenates. The Cu species in $CuFe_2O_4$ drastically inhibit the further over-oxidation process in the presence of hydroxyl radicals and yield ethanol as the major reaction products. On the other hand, the strong interaction between $CuFe_2O_4$ and CNT would promote the electrons transfer from CH_4 to catalysts, and oxygen is transferred from catalysts to CH_4 during the oxidation process [8,41-43]. Therefore, the coordination of Cu and Fe species in the $CuFe_2O_4$ and the strong interaction to CNT substrate result in highly selective conversion of CH_4 to ethanol on $CuFe_2O_4$/CNT composites.

In summary, $CuFe_2O_4$/CNT composite catalysts are synthesized *via* a co-reduction process. Ethanol with high selectivity of 82% can be directly converted from CH_4 over the $CuFe_2O_4$/CNT catalysts at low temperature of 150 °C. The unique synergistic effects of the coordination of Cu and Fe species in the $CuFe_2O_4$ as well as strong interaction to CNT substrate in $CuFe_2O_4$/CNT result in supper high selectivity for ethanol formation. This work elucidates that non-noble metals loaded on CNT can pave the way for efficient CH_4 conversion and highly valuable C_{2+} products generation.

Declaration of competing interest

The authors declare that they have no known competing financial interests or personal relationships that could have appeared to influence the work reported in this paper.

Acknowledgments

This work was financially supported by the National Natural Science Foundation of China (No. 21975163), Bureau of Industry and Information Technology of Shenzhen (No. 201901171518) and Shenzhen Science and Technology Program (No. KQTD20190929173914967). We also gratefully acknowledge the support provided by Instrumental Analysis Center of Shenzhen University (Xili Campus).

Supplementary materials

Supplementary material associated with this article can be found, in the online version, at doi:10.1016/j.cclet.2021.07.019.

References

[1] B. An, Z. Li, Y. Song, et al., Nat. Catal. 2 (2019) 709–717.
[2] Z. Lin, L. Wang, E. Zuidema, et al., Science 367 (2020) 193–197.
[3] C.T. Wang, J. Zhang, G.Q. Qin, et al., Chem 6 (2020) 646–657.
[4] C. Ma, X.J. Tan, H.J. Zhang, et al., Chin. Chem. Lett. 31 (2020) 235–238.
[5] J.C. Kang, S. He, W. Zhou, et al., Nat. Commun. 11 (2020) 827–838.
[6] B.H.T. Luk, C. Mondelli, D.G. Ferre, J.A. Stewart, J.P. Ramirez, Chem. Sov. Rev. 46 (2017) 1358–1426.
[7] H.D. Shen, Z.Y. Sun, Chem 6 (2020) 546–548.
[8] C. Hammond, M.M. Forde, M.H.A. Rahim, et al., Angew. Chem. Int. Ed. 51 (2012) 5129–5233.
[9] D.Y. Osadchii, A.I.O. Suarez, A. Szecsenyi, et al., ACS Catal. 8 (2018) 5542–5548.
[10] V.L. Sushkevich, D. Pakagin, M. Ranoccguari, J.A. Bokhoven, Science 356 (2017) 523–527.
[11] J.K. Kang, E.D. Park, Catalysts 10 (2020) 299–308.
[12] X.Z. Fang, L.H. Xia, L. Peng, et al., Chin. Chem. Lett. 30 (2019) 1141–1146.
[13] K. Narsimhan, K. Iyoki, K. Dinh, Y.R. Leshkov, ACS Cent. Sci. 2 (2016) 424–429.
[14] M.J.D. Silva, Fuel Process. Technol. 145 (2016) 42–61.
[15] S.J. Xie, S.Q. Lin, Q.H. Zhang, Z.Q. Tian, Y. Wang, J. Energy Chem. 27 (2018) 1629–1636.
[16] S.X. Bai, F.F. Liu, B.L. Huang, et al., Nat. Commun. 954 (2020) 5634–5643.
[17] N. Agarwal, S.J. Freakley, R.U. Mcvicker, et al., Science 358 (2017) 223–227.
[18] T. Li, S.J. Wang, C.S. Yu, et al., Appl. Catal. A: Gen. 398 (2011) 150–154.
[19] H.J. Kim, J. Huh, Y.W. Kwon, et al., Nat. Catal. 2 (2019) 342–353.
[20] C.C. Liu, C.Y. Mou, S.S.F. Yu, S.I. Chan, Energy Environ. Sci. 9 (2016) 1361–1374.
[21] M.O. Ross, F. Marcmillan, J.Z. Wang, et al., Science 364 (2019) 566–570.
[22] R.B. Li, M.X. Cai, Z.J. Xie, et al., Appl. Catal. B: Environ. 244 (2019) 974–982.
[23] C. Reitz, C. Suchomski, J. Haetge, et al., Chem. Commun. 48 (2012) 4471–4473.
[24] J.J. Yao, Y. Deng, S.Y. Pan, et al., J. Hazard. Mater. 415 (2021) 125551–125564.
[25] H. Wang, H. Zhou, S.Q. Li, et al., ACS Catal. 10 (2020) 10559–10569.
[26] W.X. Wang, X.K. Li, Y. Zhang, et al., Catal. Sci. Technol. 7 (2017) 4413–4421.
[27] H.L. Tang, Y. Su, B.S. Zhang, et al., Sci. Adv. 3 (2017) 1–8.
[28] M.V. Grabchenko, G.V. Manontov, V.L. Zaikovskii, et al., Appl. Catal. B: Environ. 260 (2020) 974–982.
[29] G.K. Reddy, P. Boolchand, P.G. Smirniotis, J. Phys. Chem. C 116 (2012) 11019–11031.
[30] J.L. Cao, Y. Wang, X.L. Yu, et al., Appl. Catal. B: Environ. 79 (2008) 26–34.
[31] B. Qiao, A.Q. Wang, J. Lin, et al., Appl. Catal. B: Environ. 105 (2011) 103–110.
[32] Q.L. Zhang, H.M. Wang, P. Ning, et al., Appl. Surf. Sci. 419 (2017) 733–743.
[33] E.A. Fugate, S. Biswas, M.C. Clement, et al., Nano Res. 12 (2019) 2390–2399.
[34] M. Zhu, T.C.R. Rocha, T. Lunkenbein, et al., ACS Catal. 6 (2016) 4455–4464.
[35] Y.M. Liu, D.S. Mao, J. Yu, Y.L. Zheng, X.M. Guo, Catal. Sci. Technol. 10 (2020) 8383–8395.
[36] S.L. Chu, X.P. Yan, C.H. Choi, et al., Green Chem. 221 (2020) 6540–6546.
[37] E. Amini, M.R. Rezaei, M. Sadeghinia, Chin. J. Catal. 34 (2013) 1762–1767.
[38] J.L. Gu, B.J. Zhu, R.D. Duan, et al., Catal. Sci. Technol. 10 (2020) 5525–5534.
[39] R. Polniser, M. Stolcova, M. Hronec, M. Mikula, Appl. Catal. A: Gen. 400 (2011) 122–130.
[40] Y.F. Rao, Y.F. Zhang, F.M. Han, et al., Chem. Eng. J. 352 (2018) 601–611.
[41] X.B. Huang, P. Wang, H. Zhang, et al., Eur. J. Inorg. Chem. 43 (2019) 91–97.
[42] S. Luo, J. Liu, Z.L. Wu, J. Phys. Chem. C 123 (2019) 11772–11780.
[43] X.Q. Yang, X.Y. Ma, X.L. Yu, et al., Appl. Catal. B: Environ. 263 (2020) 118297–118323.
[44] G. Herzberg, Infrared and Raman Spectra of Polyatomic Molecules, Van Nostrand, New York, 1945.
[45] N.B. Colthup, L.H. Daly, E.S. Wiberley, Introduction to Infrared and Raman Spectroscopy, Academic Press, Waltham MA, 1990, p. 51.
[46] C. Barzan, A. Piovano, M. Botavina, et al., J. Catal. 373 (2019) 173.
[47] V.J.F. Lapoutre, B. Redlich, A.F.G. Meer, et al., J. Phys. Chem. A 117 (2013) 4115.
[48] Y.L. He, F. Guo, K.R. Yang, et al., J. Am. Chem. Soc. 142 (2020) 17119.